

Controlled Reduction of $\text{LaFe}_x\text{Mn}_y\text{Mo}_z\text{O}_3/\text{Al}_2\text{O}_3$ Composites to Produce Highly Dispersed and Stable Fe^0 Catalysts: a Mössbauer Investigation

Juliana Cristina Tristão^a, Márcio César Pereira^a, Flávia Cristina Camilo Moura^b,

José Domingos Fabris^a, Rochel Montero Lago^{a*}

^aDepartamento de Química – ICEx, Universidade Federal de Minas Gerais, 31270-901 Belo Horizonte - MG, Brazil

^bDepartamento de Química – ICEB, Universidade Federal de Ouro Preto, Morro do Cruzeiro, 35400-000 Ouro Preto - MG, Brazil

Received: December 20, 2007; Revised: May 29, 2008

In this work, controlled reduction of perovskites supported on Al_2O_3 was used to prepare thermally stable nanodispersed iron catalysts based on $\text{Fe}^0/\text{La}_2\text{O}_3/\text{Al}_2\text{O}_3$. The perovskites composites $\text{LaFe}_{0.90}\text{Mn}_{0.08}\text{Mo}_{0.02}\text{O}_3$ (25, 33 and 50 wt (%))/ Al_2O_3 and $\text{LaFe}_{0.90}\text{Mn}_{0.1}\text{O}_3$ (25 wt (%))/ Al_2O_3 were prepared and characterized by XRD, BET, TPR, SEM and Mössbauer spectroscopy. XRD for unsupported perovskite showed the formation of a single phase perovskite structure. The Mössbauer spectra of the perovskites were fitted with hyperfine field distribution model for the perovskite. Supported perovskites on Al_2O_3 showed a decrease of the hyperfine field in respect to unsupported perovskite, due to decrease of particle size and dispersion of the Fe^{3+} specimens on the support. Also showed broaden lines and relaxation effects due to the small particle size. To produce the Fe^0 catalyst, the composite perovskite(25%)/ Al_2O_3 was reduced with H_2 at 900, 1000 and 1100 °C for 1 hour. XRD data indicated the formation of Fe^0 catalyst with particles sizes of ca. 35 nm. The Mössbauer spectrum showed the formation of metallic iron and doublets corresponding to species of octahedric Fe^{2+} and Fe^{3+} sites dispersed on Al_2O_3 . These catalysts showed improved stability towards sintering even upon treatment at 1000 and 1100 °C under H_2 .

Keywords: perovskite, iron, catalyst, nanoparticle

1. Introduction

Metallic iron catalysts have been investigated for many different applications, e.g. permeable reactive barriers¹, reduction of organochloro², and Fenton chemistry^{3,4}. More recently, supported iron catalysts have been intensively investigated for the synthesis of carbon nanotubes by chemical vapor deposition. For these catalysts the control of the particle size and the stability towards sintering are key factors for the catalytic performance. Different strategies have been explored recently to prepare uniformly distributed metallic catalysts for the synthesis of carbon nanotubes. These include work on zeolite templates⁵⁻¹⁰, the decomposition of soluble precursors-based molecular clusters containing Fe and Mo^{10,11} or metal carbonyl complexes $[\text{Fe}(\text{CO})_5]$ and $[\text{Mo}(\text{CO})_6]$ embedded in a long-chain carboxylic acid/amine mixture¹², and the controlled reduction of different oxides or solid oxide solutions¹³.

In this work, we have investigated a new approach to produce stable and highly dispersed Fe^0 catalysts. The Fe particles are formed by the reduction of the precursors $\text{LaFe}_x\text{Mn}_y\text{Mo}_z\text{O}_3$ perovskites dispersed on the surface of an Al_2O_3 support (Figure 1). This catalyst has been recently investigated for the synthesis of single wall carbon nanotube showing promising results¹⁴.

This preparation method shows several potential advantages: i) should allow a good control of the metallic particle size distribution, ii) should improve the thermal stability to the catalyst due to a strong matrix insulation effect (La_2O_3 and Al_2O_3 should keep Fe^0 particles well separated), iii) the precursor elements and stoichiometry can be adjusted to produce catalysts with different metals and different ratios, iv) the metals present in the precursor, e.g. Fe and Mo, should be homogeneously distributed throughout the oxide and produce well-

defined metallic particles, and v) the dispersion of the metal particle can be further controlled by the reduction conditions.

2. Experimental Procedures

Two composites were prepared: $\text{LaFe}_{0.90}\text{Mn}_{0.10}\text{O}_3$ (25 wt (%))/ Al_2O_3 and $\text{LaFe}_{0.90}\text{Mn}_{0.08}\text{Mo}_{0.02}\text{O}_3$ (25, 33 and 50 wt (%))/ Al_2O_3 . Alumina nanopowder Aldrich (<50 nm particle size and 35 $\text{m}^2\cdot\text{g}^{-1}$) was used. The perovskites were prepared by the reaction of 0.5 mol of citric acid (CA) dissolved in 2 mol of water at 60 °C, followed by the addition of 1 mmol of $\text{La}(\text{NO}_3)_3\cdot 6\text{H}_2\text{O}$ and different proportions of the other metals such as $\text{Fe}(\text{NO}_3)_3\cdot 9\text{H}_2\text{O}$, $\text{Mn}(\text{NO}_3)_2\cdot 4\text{H}_2\text{O}$ and $\text{Mo}(\text{acac})_2\text{O}_2$ (acac acetylacetonate) in order to produce the desired stoichiometry. The mixture was stirred for about 2 hours, until a clear orange solution of the stable metal-CA complexes is obtained. After the complete dissolution, 400 mmol of ethylene glycol (EG) followed by the addition of the Al_2O_3 nanopowder in amounts to obtain composites with 25, 33 and 50 wt (%) of perovskite on alumina. The suspension was continuously stirred while the temperature was slowly increased to 90 °C. This step removes the excess of water and allows the polyesterification reaction between CA and EG to be further activated. The prolonged heating at 90 °C occurs for 7 hours and resulted in a viscous orange mass¹⁵. This resin was then treated at 400-450 °C in air for 2 hours for the charring. The final product, a dark brown powder was ground and then calcined at 800 °C in air for 6 hours.

The powder XRD data were obtained in a Rigaku model Geigerflex equipment using $\text{Co K}\alpha$ radiation scanning from 10 to 80° (2 θ) at a scan rate of 4° min^{-1} . Silicon was used as an external standard.

*e-mail: rochel@ufmg.br

The crystallite sizes were determined by Scherrer's equation through the width of the Bragg reflection at half maximum. The surface area was determined by nitrogen adsorption using the BET method with a 22 cycles N_2 adsorption/desorption in an Autosorb 1 Quantachrome instrument. The transmission Mössbauer spectroscopy experiments were carried out in a spectrometer CMTE model MA250 with a $^{57}Co/Rh$ source at room temperature using $\alpha-Fe$ as a reference. The TPR (temperature programmed reduction) analysis was performed in a CHEM BET 3000 TPR using H_2 (8% in N_2) with heating rate of $10^\circ C\ min^{-1}$. The H_2 consumption was obtained after calibration of the TPR system using a CuO standard. Scanning electron microscopy (SEM) analysis was done using a Jeol JSM 840A.

The reduction of the perovskites was carried out in a quartz tube of 40 mm diameter with a batch of catalyst (50 mg) placed in the central part and heated to the reduction temperatures in the range of 900, 1000 and $1100^\circ C$ at $10^\circ C\ min^{-1}$ under an H_2/Ar flow ($100/800\ mL\ min^{-1}$) for 1 hour. The system was cooled down to room temperature under a constant H_2/Ar flow. The reduced catalyst still under H_2 flow at room temperature was completely immersed and covered with dichlorobenzene liquid to prevent oxidation by O_2 from the air.

3. Results and Discussion

The XRD patterns for the $LaFe_{0.90}Mn_{0.10}O_3(25\%)/Al_2O_3$ and $LaFe_{0.90}Mn_{0.08}Mo_{0.02}O_3(25\%)/Al_2O_3$ supported perovskites are shown in Figure 2.

The main peaks in Figure 2 are related to the perovskite structure, i.e. $LaMO_3$ ($2\theta = 26.0, 37.3, 46.2, 54.0, 61.0$ and 67.6°). A small shift in Figure 2 of the XRD peaks to lower diffraction angles have been observed due of the incorporation of the Mo into the structure. Analyses of the lattice parameters of the unsupported $LaFe_{0.90}Mn_{0.10}O_3$ and $LaFe_{0.90}Mn_{0.08}Mo_{0.02}O_3$ perovskite showed crystal structures best fitted to a pseudo-cubic arrangement^{16,17}. Figure 3 shows the XRD patterns for the $LaFe_{0.90}Mn_{0.08}Mo_{0.02}O_3$ perovskite supported on Al_2O_3 at different concentrations of perovskite. We note that lower perovskite contents produce larger peaks related to small particle size and a good dispersion on the support. Data of surface area, crystallite size and

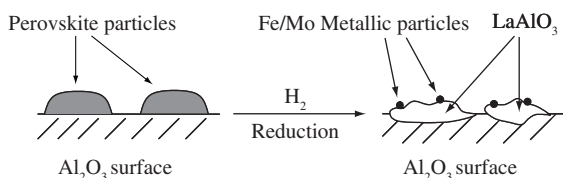


Figure 1. Formation of highly dispersed metallic particles upon reduction of the perovskite precursor dispersed on the surface of Al_2O_3 support.

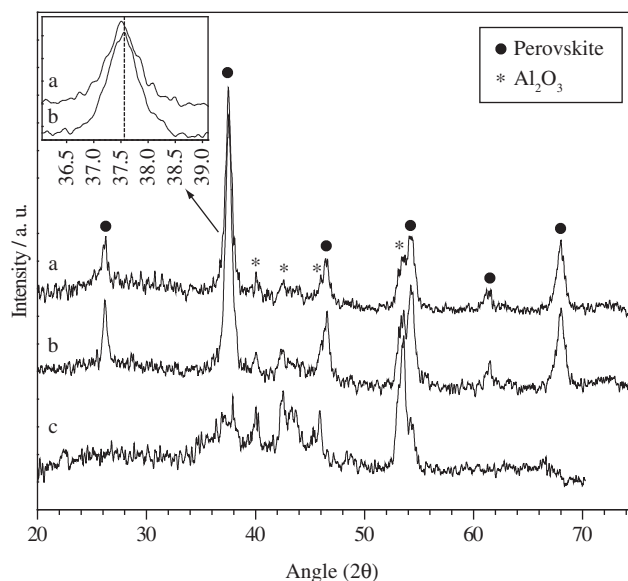


Figure 2. Powder X ray diffraction of the a) $LaFe_{0.90}Mn_{0.08}Mo_{0.02}O_3(25\%)/Al_2O_3$; b) $LaFe_{0.90}Mn_{0.10}O_3(25\%)/Al_2O_3$; and c) pure Al_2O_3 .

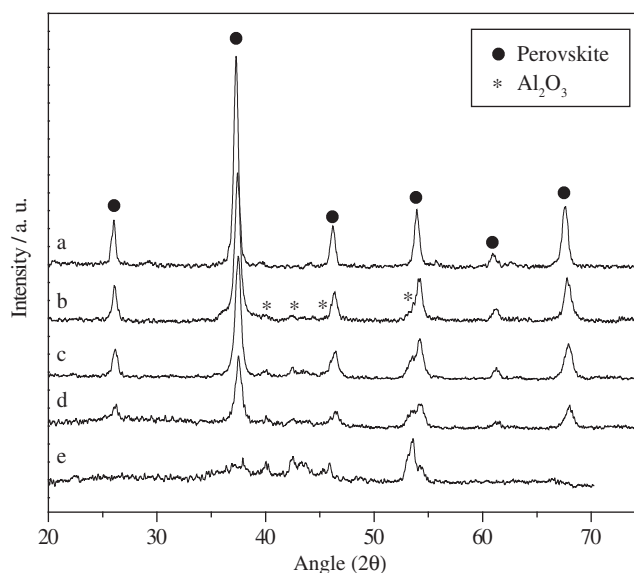


Figure 3. Powder X ray diffraction of the $LaFe_{0.90}Mn_{0.08}Mo_{0.02}O_3$ perovskite: a) pure (unsupported); b) 50 wt%; c) 33 wt%; d) 25 wt% in perovskite content; and e) Al_2O_3 .

Table 1. Surface area, average crystallite size and lattice parameter for the synthesized perovskites.

Sample	Surface area/ $m^2\cdot g^{-1}$	Crystallite size ⁽ⁱ⁾ / \AA	Lattice parameters ⁽ⁱⁱ⁾			
			a/ \AA	b/ \AA	c/ \AA	V/ \AA^3
a	11	286	3.944(1)	3.944(1)	3.944(1)	61.34(4)
b	16	202	3.935(7)	3.935(7)	3.935(7)	60.93(2)
c	22	145	3.9226(3)	3.9226(3)	3.9226(3)	60.35(3)
d	21	174	3.9159(5)	3.9159(5)	3.9159(5)	60.05(1)
e	23	165	3.9214(1)	3.9214(1)	3.9214(1)	60.30(3)
f	24	149	3.9225(2)	3.9225(2)	3.9225(2)	60.35(3)

a) $LaFe_{0.90}Mn_{0.10}O_3$; b) $LaFe_{0.90}Mn_{0.08}Mo_{0.02}O_3$; c) $LaFe_{0.90}Mn_{0.10}O_3(25\%)Al_2O_3$; d) $LaFe_{0.90}Mn_{0.08}Mo_{0.02}O_3(50\%)Al_2O_3$; e) $LaFe_{0.90}Mn_{0.08}Mo_{0.02}O_3(33\%)Al_2O_3$; and f) $LaFe_{0.90}Mn_{0.08}Mo_{0.02}O_3(25\%)Al_2O_3$. Obtained by the Scherrer equation. Obtained by the refinement of profile functions and lattice parameters with the software Fullprof_SuTe 2005 (available at <http://www-llb.cea.fr/fullweb/winplotr.htm>).

lattice parameter for the synthesized perovskite are shown in Table 1. The crystallite size found for the unsupported LaFe_{0.90}Mn_{0.08}Mo_{0.02}O₃ was 202 Å. On the other hand, for the supported perovskites significantly smaller crystallites were obtained, i.e. 174, 165 and 149 Å for LaFe_{0.90}Mn_{0.08}Mo_{0.02}O₃ 50, 33 and 25 wt(%) respectively (Table 1).

BET surface area slowly decreases from 24 to 23 and 21 m² g⁻¹ as the perovskite content increases. This results indicate that the prepared perovskite should have small surface area compared to the Al₂O₃ (ca. 35 m² g⁻¹) and contributes to decrease the composite surface area.

Mössbauer spectra of the samples (Figure 4 and 5) were fitted with a hyperfine field distribution model for octahedral Fe³⁺ coordination in the structure of the perovskite. It is possible to observe that

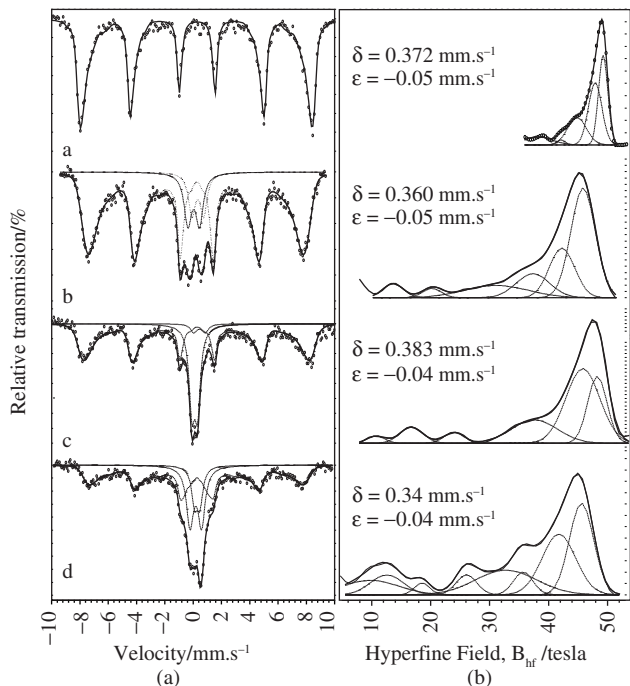


Figure 4. Mössbauer spectra of the LaFe_{0.90}Mn_{0.08}Mo_{0.02}O₃ perovskite pure and the 50, 33 and 25 wt% supported on Al₂O₃ (left side) and hyperfine field distributions (right side).

the supported perovskites (Figure 4b, 4c, 4d and 5b) show broaden lines relaxation effects, central doublets and higher range of field distribution, compared with unsupported perovskite. These effects are related to the small crystallite size and Fe³⁺ specimens highly dispersed on the support.

The Hyperfine parameters obtained from the Mössbauer spectra for the pure perovskites and supported on Al₂O₃ are shown in Table 2. The hyperfine parameters for the supported perovskites indicate the presence of two signals for octahedral Fe³⁺ specimens coordination and a decrease of the hyperfine field. These results suggest that the support promotes a strong dispersion of the Fe³⁺ specimens. The Mössbauer parameters (Table 2) of the supported perovskites 50, 33 and 25 wt% in perovskite content (Figure 4b, 4c and 4d) showed that the relative sub-spectral area of sextets were 80, 69 and 61% respectively, suggesting that higher alumina contents cause a higher dispersion of the Fe³⁺ species. The values of the quadrupole shift close to 0 corroborate with the pseudo-cubical symmetry proposal for these perovskites.

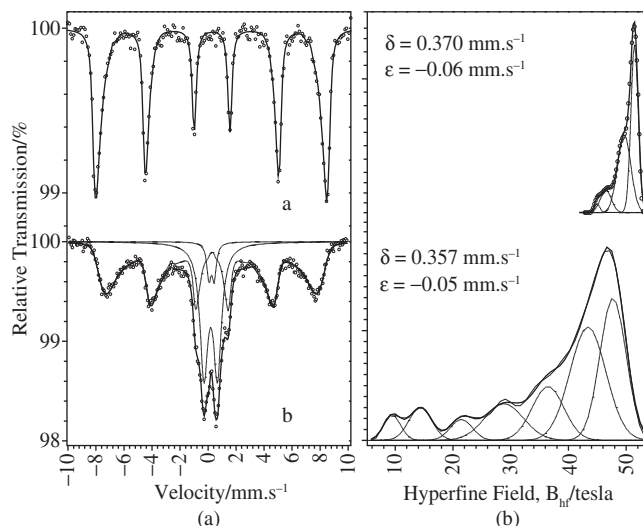


Figure 5. Mössbauer spectra of the LaFe_{0.90}Mn_{0.10}O₃ perovskite pure and the 25 wt (%) supported on Al₂O₃ (left side) and hyperfine field distribution (right side).

Table 2. Hyperfine parameters for the pure perovskites and supported on Al₂O₃ corresponding to spectra recorded at 298 K.

Sample	Site ⁵⁷ Fe	δ/mm.s ⁻¹	ε, Δ/mm.s ⁻¹	Bhf/T	Γ/mm.s ⁻¹	RA/%
a	^{VI} Fe ³⁺	0.370(3)	-0.06(1)	51.45(8)*	0.31	100 [#]
b	^{VI} Fe ³⁺	0.372(2)	-0.05(1)	51.26(8)*	0.31	100 [#]
c	^{VI} Fe ³⁺	0.357(7)	-0.05(1)	47.1(3)*	0.31	64.7 [#]
	^{VI} Fe ³⁺	0.290(4)	0.96(2)		0.69(3)	30.9
	^{VI} Fe ³⁺	0.35(1)	0.38(3)		0.35(7)	4.4
d	^{VI} Fe ³⁺	0.360(5)	-0.052(9)	47.3*	0.31	80.1 [#]
	^{VI} Fe ³⁺	0.17(3)	0.82(2)		0.60(2)	11.3
	^{VI} Fe ³⁺	0.455	0.82(2)		0.58(3)	8.6
e	^{VI} Fe ³⁺	0.384(8)	-0.05(2)	49.7*	0.31	68.5 [#]
	^{VI} Fe ³⁺	0.566(4)	0.810(9)		0.55(2)	3.4
	^{VI} Fe ³⁺	0.230(5)	0.397(9)		0.48(2)	28.1
f	^{VI} Fe ³⁺	0.336(1)	-0.04	47.1*	0.31	60.5 [#]
	^{VI} Fe ³⁺	0.275(1)	0.82(5)		0.65	26.2
	^{VI} Fe ³⁺	0.378(1)	0.40(3)		0.50(1)	13.3

a) LaFe_{0.90}Mn_{0.10}O₃; b) LaFe_{0.90}Mn_{0.08}Mo_{0.02}O₃; c) LaFe_{0.90}Mn_{0.10}O₃(25%)Al₂O₃; d) LaFe_{0.90}Mn_{0.08}Mo_{0.02}O₃(50%)Al₂O₃; e) LaFe_{0.90}Mn_{0.08}Mo_{0.02}O₃(33%)Al₂O₃; and f) LaFe_{0.90}Mn_{0.08}Mo_{0.02}O₃(25%)Al₂O₃. *Maximum hyperfine field of the distribution. [#]Relative area of the distribution. δ = isomer shift with respect to αFe; ε = quadrupole shift; Δ = quadrupole splitting; Bhf = hyperfine field; Γ = full line-width at half height; RA = relative sub-spectral area.

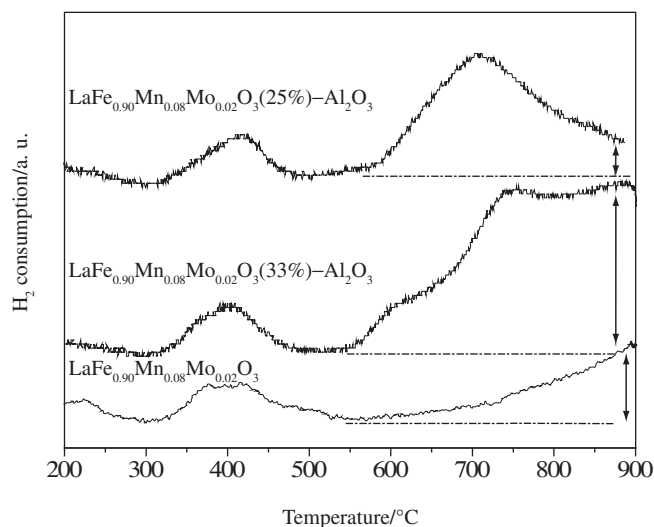
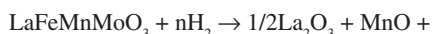


Figure 6. Temperature programmed reduction (TPR) profiles for the perovskite $\text{LaFe}_{0.90}\text{Mn}_{0.08}\text{Mo}_{0.02}\text{O}_3$ pure, 33 and 25 wt% supported on Al_2O_3 .

3.1. Controlled reduction of the prepared perovskite

Temperature Programmed Reduction (TPR) experiments were performed to investigate the reducibility of the different perovskites (Figure 6).

TPR profile for the unsupported perovskite (Figure 6) shows a set of broad peaks at 300–500 °C probably assigned to the reduction of Fe^{3+} , Mo^{4+} , Mn^{4+} and some Mn^{3+} . For the reduction at temperatures up to 500 °C the oxygen is removed from the material but the perovskite structure is still maintained. At temperatures higher 650 °C it is observed the beginning of a H_2 consumption that does not end up to 800 °C. It has been reported previously that LaFeO_3 perovskites are remarkably stable towards reduction^{18–20}. Therefore, this hydrogen consumption is likely related to the second step reduction of the Fe perovskite leading to the collapse of the perovskite structure with the formation of Fe metal, La_2O_3 and small amounts of MnO and Mo.



However, this reduction process finishes only at temperatures higher than 1000 °C under the TPR conditions. It is interesting to observe for the composite perovskite 33 wt (%) Al_2O_3 new reduction peaks at approximately 600, 730 and 880 °C (Figure 6). Also for the perovskite 25 wt (%) on Al_2O_3 a new and intense reduction peak at 700 °C appears. The presence of these new peaks at lower temperatures compared with pure perovskite suggests that the supported perovskites can be more easily reduced. This is likely related to the smaller particle size which should cause an increase in reactivity.

The influence of the reduction temperature to produce stable and highly disperse Fe^0 catalysts with particle size control was investigated. The reductions were carried out with H_2 for 1 hour at three different temperatures, i.e. 900, 1000 and 1100 °C, using the 25 wt (%) $\text{LaFe}_{0.90}\text{Mn}_{0.08}\text{Mo}_{0.02}\text{O}_3$ perovskite on Al_2O_3 .

The XRD analyses of the precursor $\text{LaFe}_{0.90}\text{Mn}_{0.08}\text{Mo}_{0.02}\text{O}_3(25\%)/\text{Al}_2\text{O}_3$ are presented in Figure 7. The results show that Fe^0 (see XRD at $2\theta = 52^\circ$) has sintered to form crystallites with average sizes of 37, 35 and 35 nm for the 900, 1000 and 1100 °C treatments, respectively. It is important to observe that the iron XRD peak is composed of different components as shown by the expanded diffractogram

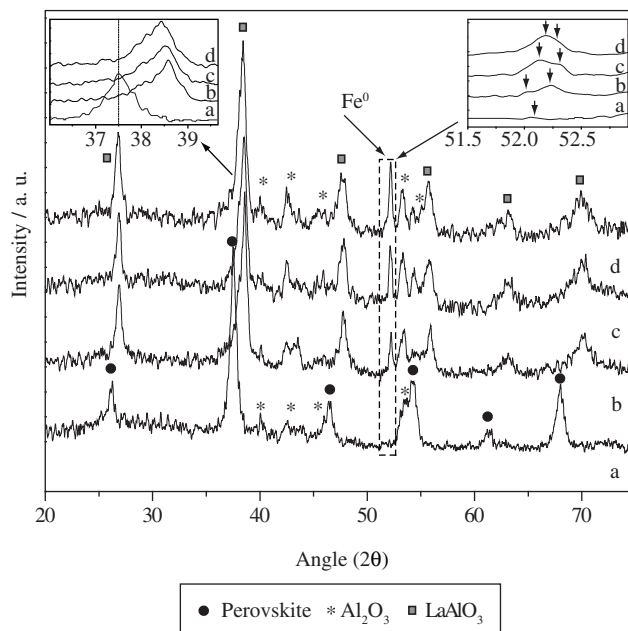
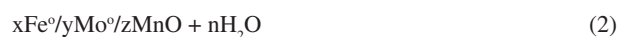
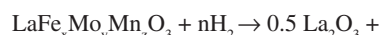


Figure 7. Powder X-ray diffraction of the perovskite $\text{LaFe}_{0.90}\text{Mn}_{0.10}\text{Mo}_{0.02}\text{O}_3(25\%)/\text{Al}_2\text{O}_3$ nanoparticles after reduction with H_2 at 900, 1000 and 1100 °C for 1 hour.

(Figure 7 detail). Therefore, the particle size estimation should be analyzed with caution.

Moreover, the XRD peaks of the perovskite after reduction have shifted by 1.0° toward higher 2θ , which is a clear indication that a new perovskite phase, probably LaAlO_3 was formed (see Figure 1). Literature data showed that La_2O_3 can react with Al_2O_3 at temperatures near 900 °C to form LaAlO_3 ^[21]. This reaction follows the steps:



Crystallite size of LaAlO_3 have been estimated by the Scherrer equation to give values of 125, 124 and 126 Å after reduction at 900, 1000 and 1100 °C, respectively.

The reduced perovskites were also studied by SEM. Figure 8, shows that the composites perovskite/ Al_2O_3 significantly changed their morphology after the reductions at different temperatures. At 900 °C the material is composed of particle agglomerates with several spaces within the particles. As the reduction temperature increased the dispersed agglomerates tend to compact and the voids tend to disappear.

Mössbauer spectra of the reduced perovskites are shown in Figures 9 and the analyses of the hyperfine parameters are given in Table 3. After the reduction of the perovskite $\text{LaFe}_{0.90}\text{Mn}_{0.08}\text{Mo}_{0.02}\text{O}_3(25\%)/\text{Al}_2\text{O}_3$ at 900 °C with H_2 (Figure 9b) it can be observed the reduction of Fe^{3+} to Fe^{2+} and Fe^0 , as showed in the Mössbauer spectra by the presence of one sextet with $\text{Bhf} = 33.1$ T corresponding to metallic iron, two doublets of octahedral Fe^{2+} and one doublet of octahedral Fe^{3+} coordination. After the reduction of the sample at 1100 °C (Figure 9c) it is possible to observe an increase in the relative area of Fe^0 and a decreasing of area of Fe^{2+} and Fe^{3+} , suggesting the reduction of these Fe species.

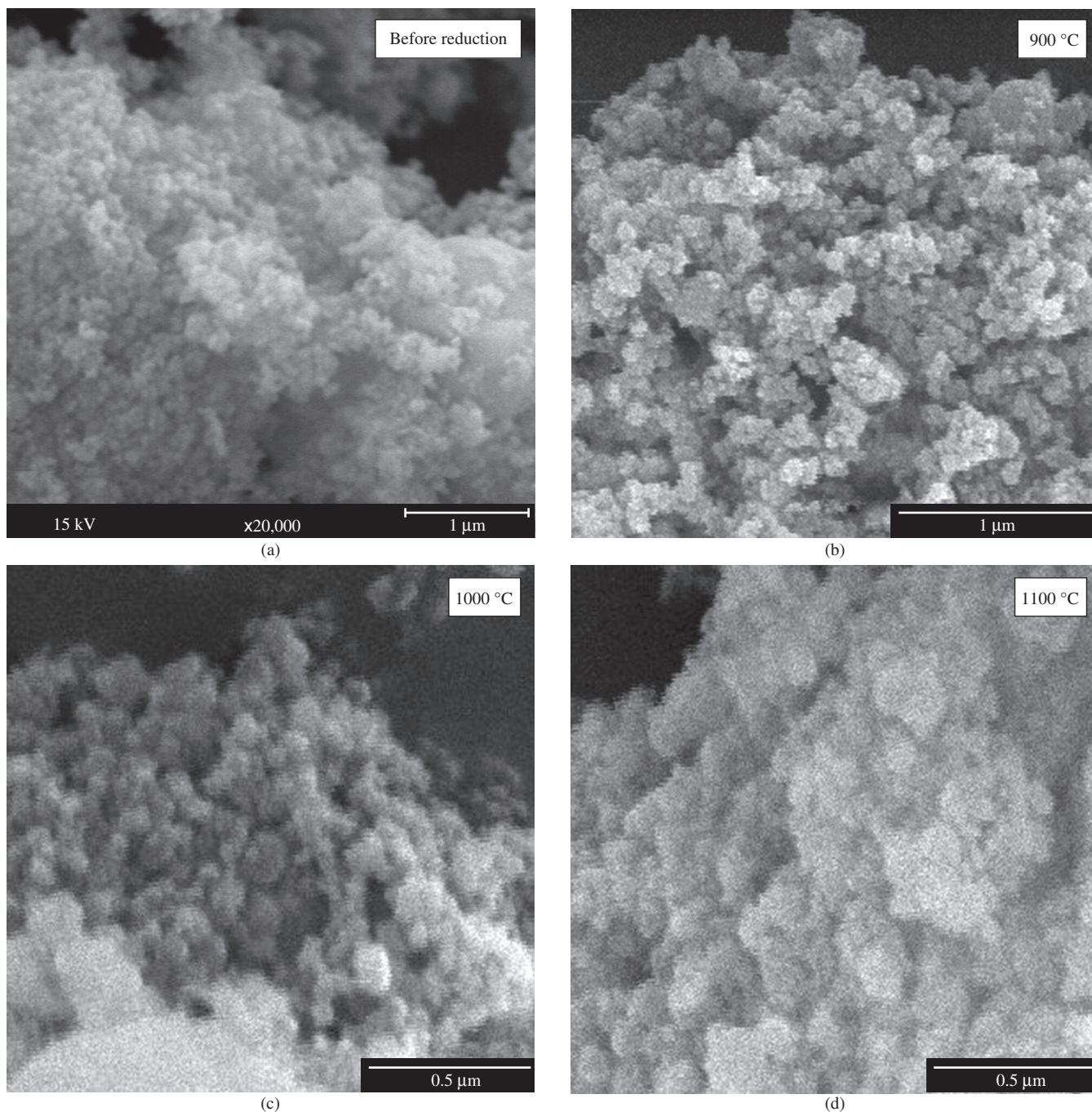


Figure 8. SEM analysis of the samples LaFe_{0.90}Mn_{0.08}Mo_{0.02}O₃(25%)/Al₂O₃ before reduction and after reduction at 900, 1000 and 1100 °C.

Table 3. Hyperfine parameters for the perovskite LaFe_{0.90}Mn_{0.08}Mo_{0.02}O₃(25%)/Al₂O₃ after reduction at 900 and 1100 °C (recorded at 298 K).

Sample	Site ⁵⁷ Fe	δ/mm.s ⁻¹	ε, Δ/mm.s ⁻¹	Bhf/T	Γ/mm.s ⁻¹	RA/%
A	Fe ⁰	-0.007(3)	0.004(7)	33.19(2)	0.37(1)	44.6(9)
Reduced at 900 °C	^{VI} Fe ³⁺	0.15(2)	0.49(4)		0.59	21.8(6)
	^{VI} Fe ²⁺	1.00(2)	0.99(4)		0.56	15.4(9)
	^{VI} Fe ²⁺	1.06(2)	1.68(4)		0.62	18.2(4)
	Fe ⁰	0.001(2)	-0.004(3)	33.00(1)	0.38(2)	75.3(9)
Reduced at 1100 °C	^{VI} Fe ³⁺	0.30(1)	0.32(2)		0.45	18.5(4)
	^{VI} Fe ²⁺	1.090(6)	1.1(1)		0.56	6.2(6)
	Fe ⁰					

A = LaFe_{0.90}Mn_{0.08}Mo_{0.02}O₃(25%)Al₂O₃, δ = isomer shift with respect to αFe; ε = quadrupole shift; Δ = quadrupole splitting; Bhf = hyperfine field; Γ = full line-width at half height; RA = relative sub-spectral area.

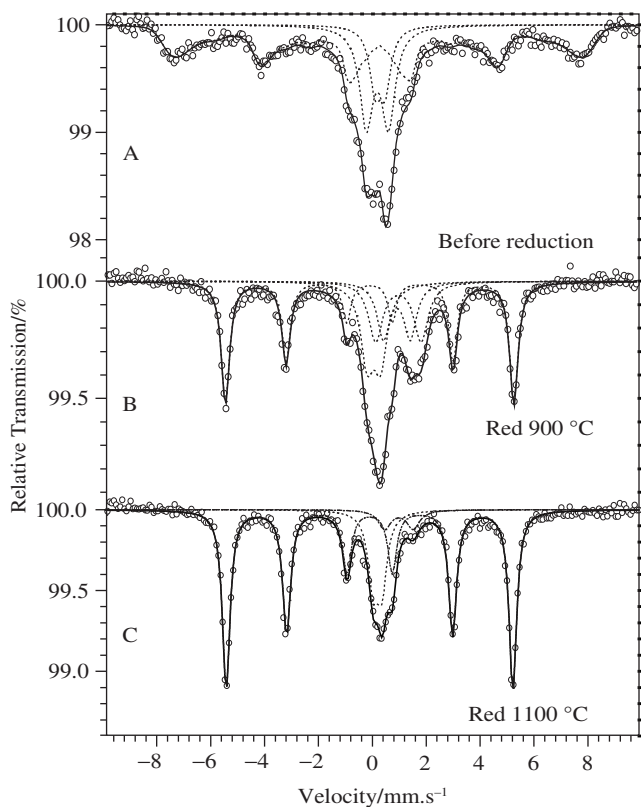


Figure 9. Mössbauer spectra at 298K of the perovskite $\text{LaFe}_{0.90}\text{Mn}_{0.08}\text{Mo}_{0.02}\text{O}_3(25\%)/\text{Al}_2\text{O}_3$ before and after reduction at 900 and 1100 °C.

4. Conclusion

In this work, composites based on the perovskites $\text{LaFe}_{0.90}\text{Mn}_{0.10}\text{O}_3$ and $\text{LaFe}_{0.90}\text{Mn}_{0.08}\text{Mo}_{0.02}\text{O}_3$ supported on Al_2O_3 were synthesized and used to prepare highly dispersed Fe^0 particles. XRD, Mössbauer spectroscopy, N_2 adsorption, TPR and SEM showed that the perovskites can be prepared on the Al_2O_3 surface with particle sizes varying from 150-180 Å. Upon reduction with H_2 under controlled conditions highly dispersed Fe^0 particles are formed. These iron catalysts showed improved stability towards sintering even under severe treatments at 1000 and 1100 °C. The production of highly dispersed and stable Fe catalyst is of considerable interest for special applications such as the synthesis of single wall carbon nanotubes.

Acknowledgements

The authors would like to thank the support of the Brazilian CNPq grants and to Prof. Richard Martel (University of Montreal) for all the support.

References

1. Khan FI, Husain T, Hejazi R. An overview and analysis of site remediation technologies. *J. Environ. Manage.* 2004; 71(2):95-122.
2. Dries J, Bastiaens L, Springael D, Agathos SN, Diels L. Competition for sorption and degradation of chlorinated ethenes in batch zero-valent iron systems. *Environ. Sci. Technol.* 2004; 38(10):2879-2884.

3. Moura FCC, Araujo MH, Ardisson JD, Macedo WAA, Albuquerque AS, Lago RM. Investigation of the solid state reaction of LaMnO_3 with Fe^0 and its effect on the catalytic reactions with H_2O_2 . *J. Braz. Chem. Soc.* 2007; 18(2):322-329.
4. Moura FCC, Oliveira GC, Araujo MH, Ardisson JD, Macedo WAA, Lago RM. Highly reactive species formed by interface reaction between Fe^0 iron oxides particles: An efficient electron transfer system for environmental applications. *Appl. Catal. A* 2006; 307(2):195-204.
5. Yang YH, York JD, Xu JQ, Lim S, Chen Y, Haller GL. Statistical design of C10-Co-MCM-41 catalytic template for synthesizing smaller-diameter single-wall carbon nanotubes. *Microp. Mesop. Mater.* 2005; 86(1-3):303-313.
6. Chen Y, Ciuparu D, Yang YH, Lim S, Wang C, Haller GL, Pfefferle LD. Single-wall carbon nanotube synthesis by CO disproportionation on nickel-incorporated MCM-41. *Nanotechnology* 2005; 16(7):S476-S483.
7. Amama PB, Lim S, Ciuparu D, Yang YH, Pfefferle L, Haller GL. Synthesis, characterization, and stability of Fe-MCM-41 for production of carbon nanotubes by acetylene pyrolysis. *J. Phys. Chem. B* 2005; 109(7):2645-2656.
8. Konya Z, Vesselenyi I, Kiss J, Farkas A, Oszko A, Kiricsi I. XPS study of multiwall carbon nanotube synthesis on Ni-, V-, and Ni-, V-ZSM-5 catalysts. *Appl. Catal. A* 2004; 260(1):55-61.
9. Urban M, Konya Z, Mehn D, Zhu J, Kiricsi I. Mesoporous silicates as nanoreactors for synthesis of carbon nanotubes. *Phys. Chem. Comm* 2002:138-141.
10. Huang SM, Fu Q, An L, Liu J. Growth of aligned SWNT arrays from water-soluble molecular clusters for nanotube device fabrication. *PCCP* 2004; 6(6):1077-1079.
11. An L, Owens JM, McNeil LE, Liu J. Synthesis of nearly uniform single-walled carbon nanotubes using identical metal-containing molecular nanoclusters as catalysts. *J. Am. Chem. Soc.* 2002; 124(46):13688-13689.
12. Li Y, Liu J, Wang YQ, Wang ZL. Preparation of monodispersed Fe-Mo nanoparticles as the catalyst for CVD synthesis of carbon nanotubes. *Chem. Mater.* 2001; 13(3):1008-1014.
13. Flahaut E, Govindaraj A, Peigney A, Laurent C, Rousset A, Rao CNR. Synthesis of single-walled carbon nanotubes using binary (Fe, Co, Ni) alloy nanoparticles prepared in situ by the reduction of oxide solid solutions. *Chem. Phys. Lett.* 1999; 300(1-2):236-242.
14. Moura FCC, Tristão JC, Lago RM, Martel R. $\text{LaFe}_x\text{Mo}_y\text{Mn}_z\text{O}_3$ perovskite as catalyst precursors for the CVD synthesis of carbon nanotubes. *Catal. Today* 2008; 133:846-854.
15. Popa M, Frantti J, Kakihana M. Lanthanum ferrite LaFeO_3 +d nanopowders obtained by the polymerizable complex method. *Solid State Ionics.* 2002; 154:437-445.
16. Náráy-Szabó StV. Die Strukturen von Verbindungen ABO_3 "Schwesterstrukturen". *Naturwissenschaften* 1943; 31(39-40):466.
17. Islam MS, Cherry M, Catlow CRA. Oxygen diffusion in LaMnO_3 and LaCoO_3 perovskite-type oxides: A molecular dynamics study. *J. Solid State Chem.* 1996; 124(2):230-237.
18. Berry FJ, Ren X, Marco JF. Reduction properties of perovskite-related rare earth orthoferrites. *Czechoslovak J. Phys.* 2005; 55(7):771-780.
19. Spinicci R, Tofanari A, Delmastro A, Mazza D, Ronchetti S. Catalytic properties of stoichiometric and non-stoichiometric LaFeO_3 perovskite for total oxidation of methane. *Mater. Chem. Phys.* 2002; 76(1):20-25.
20. Zhong ZY, Chen KD, Ji Y, Yan QJ. Methane combustion over B-site partially substituted perovskite-type LaFeO_3 prepared by sol-gel method. *Appl. Catal. A* 1997; 156(1):29-41.
21. Key TS, Crist B. Metastable states in alumina-rich La_2O_3 : Al_2O_3 and Nd_2O_3 : Al_2O_3 . *J. Am. Ceram. Soc.* 2005; 88(1):191-195.